DRAFT (6/14/04)

Assessment of PARCS Core Simulator for ACR-700 Application

Purdue University

T. Downar

C. Cotton D. Lee

Prepared for

Information Systems Laboratory (ISL)

Task 2
Contract # 4421-100

June 14, 2004

I. INTRODUCTION

The objective of this letter report is to summarize the work performed under Task 2 which was to investigate the applicability of the PARCS three dimensional neutronics core simulator to the ACR-700 and to identify specific modifications to PARCS necessary to perform coupled TRACE/PARCS analysis of the ACR-700. Since PARCS was originally designed for LWR analysis, there are some obvious coding modifications that will be necessary to describe the functionality of the ACR. However, the applicability to the ACR of the LWR neutronics methods currently used in PARCS is less obvious and therefore some background analysis was performed as part of this Task. A sequence of calculations was performed on both the CANDU-6 and the ACR-700, first with the integral transport lattice code HELIOS [Stammler, 1995] and then with the PARCS [Downar, 2002] code using HELIOS cross sections. The calculations at each level provided insight about the impact of various approximations used in PARCS to solve the neutron transport equation, and the adequacy of these approximations for simulating the neutronics behavior of the ACR-700.

The report is organized as follows. Section II summarizes the background calculations performed in support of the analysis. Section II.A reviews single lattice calculations for the CANDU-6 lattice and the CANFLEX ACR-700 lattice, to include an analysis of the important differences in the neutronics behavior of the CANDU-6 and CANFLEX lattices upon coolant voiding. Section II.B reviews the results of 2x2 lattice calculations, first with HELIOS and then PARCS with HELIOS single assembly cross sections. One of the primary purposes of this investigation was to begin isolating the impact of the various approximations used in the PARCS calculation (e.g. number of energy groups, transport vrs. diffusion, cross section homogenization, etc). This section will also provide a neutronics analysis of the checkerboard voided configuration. Section II.C reports the results of extending the analysis to three-dimensional "mini-cores", first 3x4 fuel assembly arrays for the CANDU-6 for which results were previously reported in the literature [Sarsour, 2002], [Rahnema, 2000], and then 4x4 arrays for the ACR-700 which were proposed by CNSC [Serghuita, 2004a]. Finally, section II.D reports results of preliminary PARCS full core 2-D and 3-D calculations. The important conclusions of the analysis are summarized in Section III, which also discusses the various modifications to PARCS proposed for ACR analysis. Section III.A reviews the proposed code functional modifications and Section III.B reviews the proposed code methods modifications.

2. BACKGROUND ANALYSIS

In support of the pre-application review process, the NRC Office of Nuclear Regulatory Research (RES) applied the Phenomena Identification and Ranking Technique (PIRT) to the ACR [Diamond, 2004]. Some of the calculations performed here provided background for that study. The objective of the PIRT exercise was to identify potentially important safety issues as they apply to the ACR-700 design and to provide guidance for additional development of analytical tools. The PIRT was organized into thermal-hydraulic, nuclear, and severe accident analysis areas. Of specific interest to the work here was the nuclear analysis PIRT.

There were two scenarios selected for consideration by the nuclear analysis panel. The first scenario which is of particular interest to the Coolant Void Reactivity (CVR) was a large loss-of-coolant accident (LOCA) due to either an inlet or outlet header break which is large enough to initially void half the channels. This would create a checkerboard pattern of voiding in the plane perpendicular to the direction of flow and only at a later time would all the channels become completely voided. The second scenario of interest to the PIRT nuclear analysis panel was also a LOCA, however, in this case the interest was not in particular scenarios. Rather the interest was in all LOCAs since they have in common the need to know the decay heat level throughout the core and hence, also the initial power distribution.

In the PIRT analysis, the calculation of the CVR and the power distribution was broken into three components: reactor conditions, core simulation (neutronics and thermal-hydraulics), and lattice physics. The results of the PIRT analysis indicate that there are gaps in all three elements of the calculation, however, the results of the core simulation are most relevant to the work here. Specifically, the phenomenon in the Nuclear PIRT with the largest discrepancy between importance and knowledge level was related to the homogenization of the cross sections for use in the PARCS code. The report noted that homogenization errors in predicting the CVR are particularly pronounced where leakage effects are important, such as when the core is voided and leakage from peripheral channels to the adjacent reflector regions provides important negative reactivity effects, or when the core is voided in a checkerboard pattern and internodal leakage is important. A discussion of homogenization and possible methods improvements in PARCS are discussed in section III.B. The following subsections will first review the sequence of calculations performed as part of this Task to assess possible methods deficiencies, such as homogenization.

II.A Single Assembly Calculations

The ACR-700 CANFLEX lattice is an evolution of the CANDU-6 lattice in order to achieve a negative coolant void reactivity (CVR) in the ACR-700 [Ovenes, 2002], [AECL, 2003b]. Among the alterations from the CANDU-6 lattice are a reduction in the fuel pitch, a change from heavy to light water coolant, and a change from a 37-element CANDU-6 fuel bundle containing natural uranium to the 43 element CANFLEX fuel bundle containing slightly enriched uranium (2.1wt% U-235) in the outer rods and a natural uranium center rod containing a burnable poison (7.5 wt% Dy). AECL calculations indicate that these modifications will provide the ACR-700 with a negative coolant void reactivity, unlike the previous CANDU design [Whitlock, 1995] [Ovanes, 2002].

In order to benchmark the codes used in the analysis and to achieve a better understanding of the physics issues related to the coolant void reactivity, models of the CANDU-6 and CANFLEX fuel lattices were constructed using the Scandpower/Studsvik lattice code HELIOS with a 47 group library. Models were constructed of both the CANDU-6 and ACR-700 fuel lattices using specifications provided by AECL [Whitlock, 1995], [Ovanes, 2002], [AECL, 2003a]. The basic structure of each fuel lattice is compared in Figure 1.

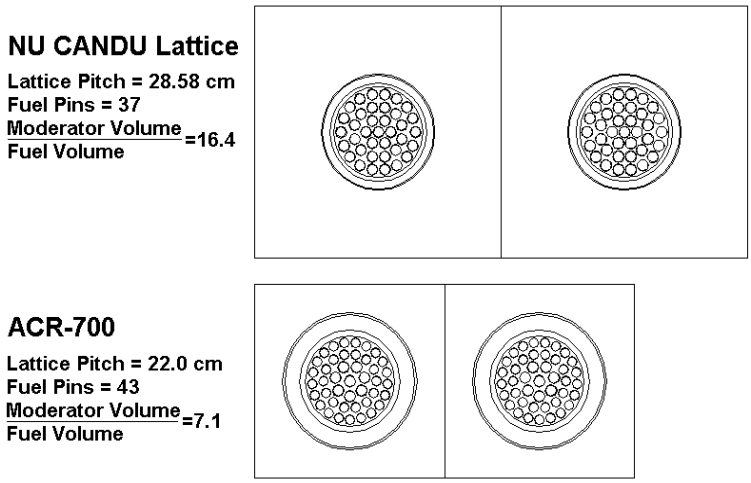

Fig. 1. CANDU-6 and ACR-700 Fuel Lattices

Calculations simulating a 0% voiding and instantaneous 100% voiding of the coolant were performed for both fuel designs. Calculations were performed at 0 GWd/t burnup for fresh and equilibrium Xe/Sm conditions, as well as at a burnup of 10 GWd/t. The CVR was computed using:

$$\Delta\rho = \left(\frac{1}{k_{0\%void}} - \frac{1}{k_{100\%void}} \right) \times 1000mk \qquad (1)$$

Comparison of the CVR for the CANDU-6 and CANFLEX/ACR Lattices

A sequence of calculations was first performed in order to understand the impact on the CVR of the various design changes during the evolution of the CANDU-6 lattice to the CANFLEX lattice. In this first set of calculations, only a fully voided lattice was analyzed. As indicated in Table 1, a CVR of +17.1 mk was predicted by HELIOS for the CANDU-6 lattice, which agrees well with the published AECL results at the same conditions [Whitlock, 1995]. A sequence of four calculations were then performed with various design changes to the CANDU-6 lattice. First the CANDU-6 lattice pitch was retained, but with 43 CANFLEX fuel pins at 2.1% enrichment and Light Water replacing the Heavy Water Coolant. This resulted in an increase in the CVR to +39.5mk. From this design, the lattice pitch was then reduced to the ACR-700 specifications, resulting in a significant decrease in the CVR from +39.5 mk to +4.7 mk. The Dysprosium Burnable Absorber was then added to the central pin which made the CVR negative at -1.3mk, which agrees well with the AECL published results [Ovanes, 2002], [AECL, 2003b]. One final calculation was performed in which the lattice was depleted to 10 Gwd/t, which made the CVR even more negative at -5.6 mk. As will be shown in section II.D, the core leakage will add an additional few mk of negative reactivity to the CVR.

The sequence of calculations here indicates that the dominant design changes contributing to the negative CVR were the change in the pitch from the CANDU to the ACR CANFLEX lattice and the addition of the Dysprosium Burnable Absorber. A detailed analysis of the negative contribution to the reactivity from specific Dysprosium isotopes was performed and the results are summarized in Appendix A.

Table 1 Reactor Effect of Various Design Changes in the CANDU-6 Lattice

Lattice Pitch	Assembly Type	Fuel Type	BA	CVR [mk]	BU [GWd/t]	COOLANT
CANDU	37-Element	Natural	No	+17.1	0	D_2O
CANDU*	CANFLEX	Natural / 2.1% Enriched	No	+39.5	0	H_2O
ACR-700	CANFLEX	Natural / 2.1% Enriched	No	+4.7	0	H_2O
ACR-700	CANFLEX	Natural / 2.1% Enriched BA Dy 7.5%	Yes	-1.3	0	H_2O
ACR-700	CANFLEX	Natural / 2.1% Enriched BA Dy 7.5%	Yes	-5.6	10	H_2O

A more detailed analysis was then performed to understand the physical basis for the neutronics differences that occur during the voiding of the CANDU-6 and CANFLEX lattices. The changes in the bundle average energy spectrum that occur due to 100% voiding of the CANDU and CANFLEX bundles are shown in Figure 2 for the zero burnup condition without equilibrium Xe/Sm. Consistency in the 0% and 100% coolant voided spectra was achieved by preserving the total neutron source in both calculations. Figure 2 illustrates that voiding the CANDU-6 fuel lattice results in energy shifts for the fast, epithermal, and thermal parts of the neutron energy spectrum. Upon voiding, the thermal energy spectrum shifts to a lower energy range corresponding to a larger thermal fission cross-sections in U-235 and an increase in the thermal utilization, the epithermal spectrum increases leading to an increase in the epithermal resonance escape probability, and the fast spectrum is shifts to a harder energy range corresponding to increased fast fission cross-sections in U-238. The spectral shifts occurs because most of the neutron moderation takes place within the much larger moderator region of the fuel lattice that is not affected during coolant voiding. Additionally, in the unvoided lattice there is a significant amount of upscattering as neutrons move from the moderator to the much hotter coolant region. During voiding, the coolant density is reduced and the upscattering effect is reduced, resulting in a positive reactivity. At the same time, the fast neutrons generated within the fuel are not being moderated as effectively after voiding due to the reduction in coolant density, which increases fast fission and results in a positive reactivity.

A comparison of the spectral changes of the CANDU-6 and CANFLEX lattices in Figure 2 indicates that there is a reduction in the thermal flux and an increase in the epithermal flux in the ACR-700 lattice upon coolant voiding. This flux shift occurs primarily because of the reduced lattice pitch in the CANFLEX lattice and the loss of light water coolant which has a better down scattering ability compared to heavy water in the CANDU-6 lattice. As will be seen in the next section, the increased epithermal flux in the CANFLEX lattice leads to a significant increase in the resonance absorption upon voiding and a large negative contribution to the CVR.

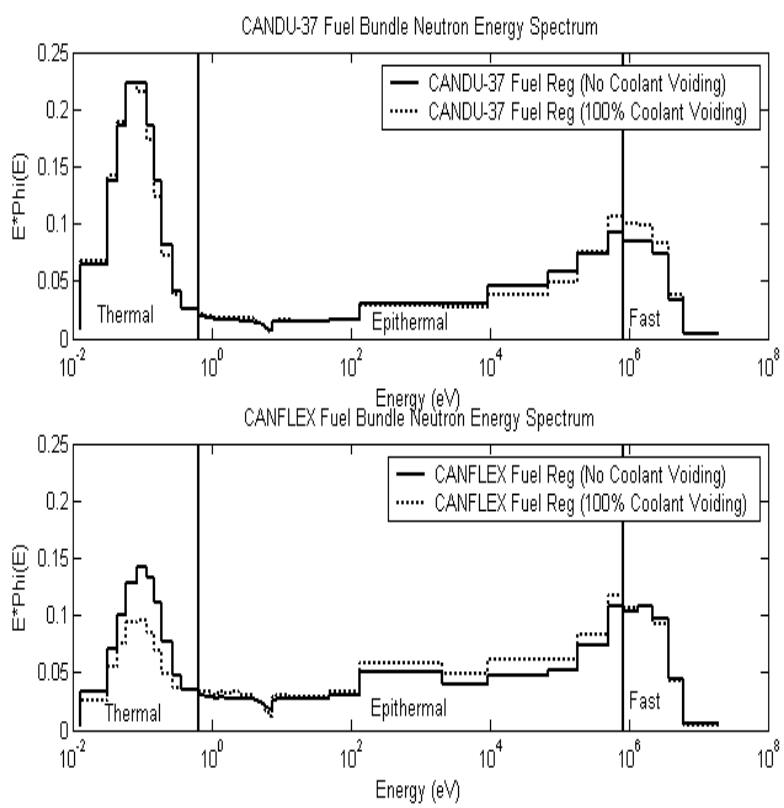

Figure 2 Comparison of Neutron Energy Spectra (0-GWd/t)

The specific contributions to the reactivity changes for both the CANDU-6 and ACR CANFLEX lattices were analyzed using the reaction rate edits from HELIOS to construct each of the factors in the familiar four factor formula. This approach is consistent with the work reported by Whitlock [Whitlock, 1995] for a typical CANDU fuel lattice. Consistent with Whitlock's approach, the resonance escape probability in the four factor formula was separated into an epithermal and fast factor to more clearly isolate the physics of coolant voiding. The reaction rates were edited with the following energy group structure: 0 eV to .625 eV (Thermal), .625 eV to .821 MeV (Epithermal), and .821 MeV to 10 MeV (Fast). The factors evaluated include the reproduction factor (η), fuel utilization factor *(f),* fast fission factor *(ε)*, and the resonance escape probability *(p*), where the two components of the resonance escape are noted as the epithermal escape probability (p_E) and the fast escape probability (p_F). The specific contributions of each parameter to the overall reactivity change are calculated using the following formulas, where 1=cooled and 2=voided states:

$$\Delta\rho_\eta = \left(\frac{1}{\eta_1 f_1 \varepsilon_1 p_{E1} p_{F1}} - \frac{1}{\eta_2 f_1 \varepsilon_1 p_{E1} p_{F1}}\right) \times 1000mk \quad (2)$$

$$\Delta\rho_f = \left(\frac{1}{\eta_2 f_1 \varepsilon_1 p_{E1} p_{F1}} - \frac{1}{\eta_2 f_2 \varepsilon_1 p_{E1} p_{F1}}\right) \times 1000mk \quad (3)$$

$$\Delta\rho_\varepsilon = \left(\frac{1}{\eta_2 f_2 \varepsilon_1 p_{E1} p_{F1}} - \frac{1}{\eta_2 f_2 \varepsilon_2 p_{E1} p_{F1}}\right) \times 1000mk \quad (4)$$

$$\Delta\rho_{p_E} = \left(\frac{1}{\eta_2 f_2 \varepsilon_2 p_{E1} p_{F1}} - \frac{1}{\eta_2 f_2 \varepsilon_2 p_{E2} p_{F1}}\right) \times 1000mk \quad (5)$$

$$\Delta\rho_{p_F} = \left(\frac{1}{\eta_2 f_2 \varepsilon_2 p_{E2} p_{F1}} - \frac{1}{\eta_2 f_2 \varepsilon_2 p_{E2} p_{F2}}\right) \times 1000mk \quad (6)$$

$$CVR = \Delta\rho_\eta + \Delta\rho_f + \Delta\rho_\varepsilon + \Delta\rho_{p_E} + \Delta\rho_{p_F} \quad (7)$$

The specific reactivity components contributing to the overall coolant void reactivity for both 0% coolant voided and the 100% coolant voided conditions are provided in Table 2. A comparison of the HELIOS results and those reported by Whitlock are provided in the first two columns. It should be noted that the positive CVR for the CANDU-6 fuel is composed of a summation of relatively small contributions from each of the four factor parameters. In contrast, the four factors for CANFLEX/ACR-700 lattice are much larger in magnitude and the small negative reactivity is the result of differences in large positive and negative four factor components.

Table 2 Void Reactivity Components

	WIMS AECL*	HELIOS 1.8			
	CANDU-6	CANDU-6		ACR – 700	
	0 MWd/t	0 MWd/t (Fresh)	0 MWd/t (Equil-Xe)	0 MWd/t (Fresh)	0 MWd/t (Equil-Xe)
	[mk]	[mk]	[mk]	[mk]	[mk]
$\Delta\eta$	+1.8	+1.4	+1.1	-5.2	-6.1
Δf	+3.3	+4.3	+4.5	+40.0	+40.1
$\Delta\varepsilon$	+4.4	+4.0	+4.3	+35.7	+38.4
Δp_E	+9.9	+10.2	+10.6	-68.3	-70.6
Δp_F	-3.2	-2.4	-2.5	-3.8	-3.9
CVR	+16.3	+17.5	+17.9	-1.6	-2.0

*Whitlock, 1995

The reproduction factor (η) provides a positive reactivity contribution in the CANDU-6 lattice because of the shift in the thermal flux to a range with a larger thermal fission cross-section. However in the ACR-700 lattice, there is a net reduction in the thermal neutron flux and thermal fissions resulting in a negative reactivity contribution.

The fuel utilization factor *(f)* provides a positive reactivity contribution in the CANDU-6 lattice because of the shift of the thermal spectrum to a range with a larger thermal fission and smaller macroscopic capture cross-section. In the ACR-700 lattice, there is a much larger positive contribution due primarily to the reduction in the density of the light water, which is a stronger neutron absorber and comprises a much larger fraction of the lattice than the heavy water coolant in the CANDU-6 lattice.

The fast fission factor *(ε)* provides a positive reactivity contribution in the CANDU-6 lattice due to the shifting of the fast neutrons to a range with a larger fast fission cross-section. In the ACR-700 lattice, there is a positive reactivity contribution due to spectral hardening. However, the resulting increase is much larger in magnitude due to the much larger increase in the epithermal and fast neutron flux resulting from the reduced moderator to fuel volume ratio.

The epithermal resonance escape probability *(p_E)* provides a positive reactivity contribution in the CANDU-6 lattice because of the large amount of moderator which will still provide sufficient moderation even upon full coolant voiding and thereby redistribute the epithermal neutrons to the moderator region so that fewer neutrons experience the resonance absorption by U-238. However, in the ACR-700 lattice, the effect of the epithermal resonance escape probability *(p_E)* is large and negative because, as shown in Figure 2, there is a large increase of epithermal and fast neutron fluxes resulting from the reduced moderator to fuel volume ratio. Upon coolant voiding, there is a large negative reactivity contribution due to the spectral hardening and increased resonance absorption. As indicated in Table 2, this is the single most important effect providing a negative CVR for the fully voided CANFLEX lattice.

Partial Voiding of the CANFLEX Lattice

The single channel analysis was then extended to an analysis of partial voiding of the CANFLEX lattice. Two sets of calculations were performed in order to compare the difference in homogeneous and heterogeneous voiding of the lattice. In the first set of calculations, the coolant was removed from the channel by uniformly reducing the coolant density from 0% to 100% in the lattice. In the second set of calculations, heterogeneous voiding of the lattice was simulated by removing coolant from the channel in sequential $1/7^{th}$ slices of the lattice. As shown in Figure 3, the CANFLEX lattice is $1/7^{th}$ symmetric which made it possible to remove the coolant sequentially from 0/7 to 7/7 in 1/7 increments. Even though such a voiding scenario is non-physical, it provides neutronics insight which contribute to the understanding of the actual checkerboard voided arrangements which will be analyzed in the following section. As in the previous section, reaction rate edits were extracted from HELIOS to construct each factor in the four factor formula for both the homogeneous and heterogeneous cases. All calculations were performed for fresh fuel (0 Gwd/t). The total reactivity change observed in the single channel model for reducing the coolant homogeneously and heterogeneously (sequential $1/7^{th}$ slices) are shown in Figure 4.

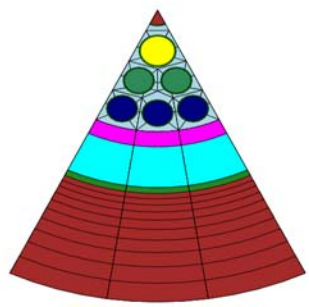

Figure 3 $1/7^{th}$ Symmetric HELIOS Model of CANFLEX Assembly

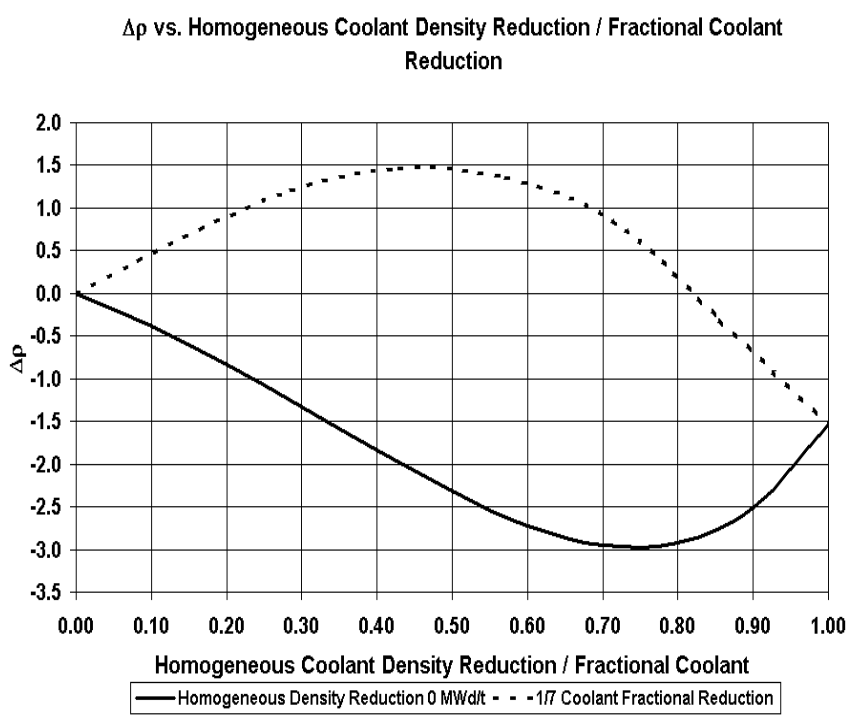

Fig. 4 Comparison of Reactivity Changes for Homogeneous vrs Heterogeneous Coolant Changes

As indicated in Figure 4, the CVR from homogeneous coolant voiding is always negative. As the coolant density is reduced, the CVR becomes more negative until about a 75% reduction in coolant density has taken place. After about a 75% reduction in the coolant density, the reactivity change increases, but remains negative. Conversely, the heterogeneous voiding is initially positive and only becomes negative after about 80% of the coolant is removed. The results of this plot suggest that there are significant spatial heterogeneous effects that can lead to a positive reactivity change upon partial voiding of the lattice.

The four factor analysis was applied to both the homogeneous and heterogeneous partial voiding cases. The components of the reactivity which contribute to the overall reactivity change for 10% increments of the homogeneous voided states are shown in Table 3 and Table 4 lists the component of the reactivity change for 1/7th increments of the heterogeneous voided states.

Table 3 Reactivity Components for Homogeneous Reduction in Coolant Reactivity

Four Factor Component	0.10	0.20	0.30	0.40	0.50	0.60	0.70	0.80	0.90	1.00
$\Delta\eta$	-0.3	-0.6	-0.9	-1.3	-1.7	-2.3	-2.8	-3.5	-4.3	-5.2
Δf	3.6	7.3	11.0	14.9	18.7	22.7	26.8	31.0	35.4	40.0
$\Delta\varepsilon$	2.8	5.7	8.8	12.0	15.4	19.1	22.8	26.9	31.2	35.7
Δp_E	-6.2	-12.6	-19.3	-26.1	-33.1	-40.2	-47.6	-54.5	-61.5	-68.3
Δp_F	-0.2	-0.5	-0.9	-1.3	-1.5	-2.0	-2.8	-2.7	-3.2	-3.8
Sum	-0.3	-0.8	-1.3	-1.8	-2.2	-2.7	-3.6	-2.9	-2.5	-1.7

Table 4 Reactivity Components for Heterogeneous Reduction in Coolant Reactivity

Fract	1/7	2/7	3/7	4/7	5/7	6/7	1
$\Delta\eta$	-1.1	-2.0	-2.7	-3.4	-4.2	-4.8	-5.2
Δf	6.0	11.7	17.2	22.8	28.6	34.4	40.0
$\Delta\varepsilon$	3.9	8.2	12.7	17.6	23.1	29.1	35.7
Δp_E	-7.8	-15.7	-24.2	-33.7	-44.1	-55.9	-68.3
Δp_F	-0.5	-1.0	-1.5	-2.0	-2.6	-3.2	-3.8
Sum	0.7	1.3	1.5	1.3	0.8	-0.4	-1.6

As indicated in the Tables, the two most dominant components are the thermal utilization and the resonance escape probability. These two components are plotted separately for the homogeneous and heterogeneous cases in Figure 5.

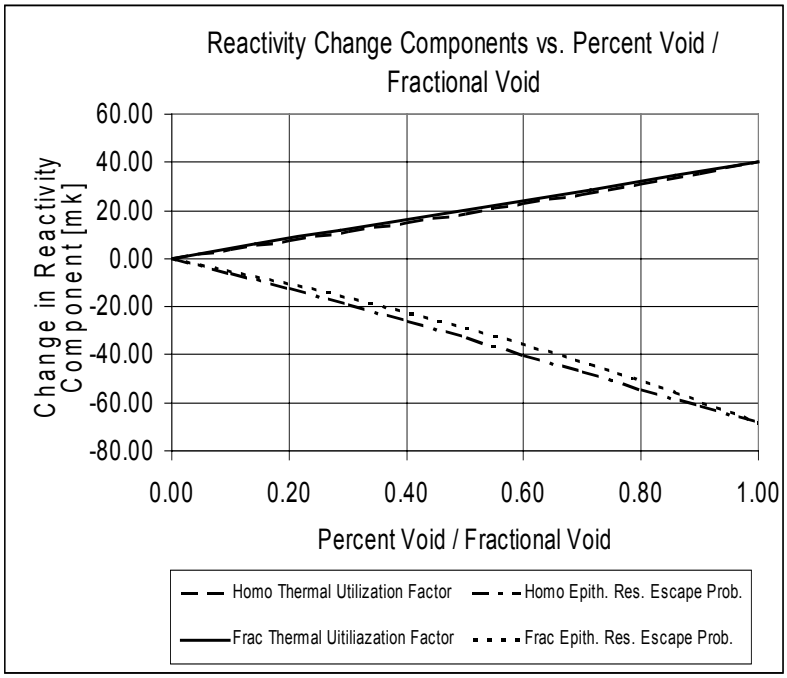

Fig. 5 Comparison of Reactivity Components from Tables 3 and 4

As indicated in Figure 5, when the coolant is removed the change in the fuel utilization factor becomes increasingly positive and the change in the epithermal resonance escape probability becomes increasingly negative for both homogeneous and heterogeneous cases. The increasingly positive change in thermal utilization with increased voiding is primarily due to the reduction in parasitic neutron absorption in hydrogen as the coolant is removed, while the increasingly negative change in resonance escape probability with increased voiding is the result of increased resonance absorption in the fuel as the spectrum hardens as the coolant is removed.

As indicated in Figure 5, the change in the thermal utilization is similar for both homogeneous and heterogeneous cases. However, there is an important difference in the change in the resonance escape probability for the homogeneous and heterogeneous cases as the coolant is removed. The decrease in the resonance escape probability in the heterogeneous case is less negative during intermediate voided states, and as was shown in Figure 4, leads to an overall positive CVR during partial voiding. The physical reasons for this behavior can be attributed to a spatial self shielding effect in the heterogeneous voided lattice that will be more clearly demonstrated using the actual checkerboard voiding configuration in the 2x2 assembly case in the next section.

II.B 2x2 CANFLEX Assembly Calculations

The next sequence of calculations was to extend the single lattice ACR to a 2x2 array in order to investigate the impact of checkerboard voiding and to begin evaluating the impact of approximations used in the PARCS calculation. A 2x2 HELIOS model was constructed as shown in Figure 6 and the conditions used for the 2x2 analysis are shown in Table 5.

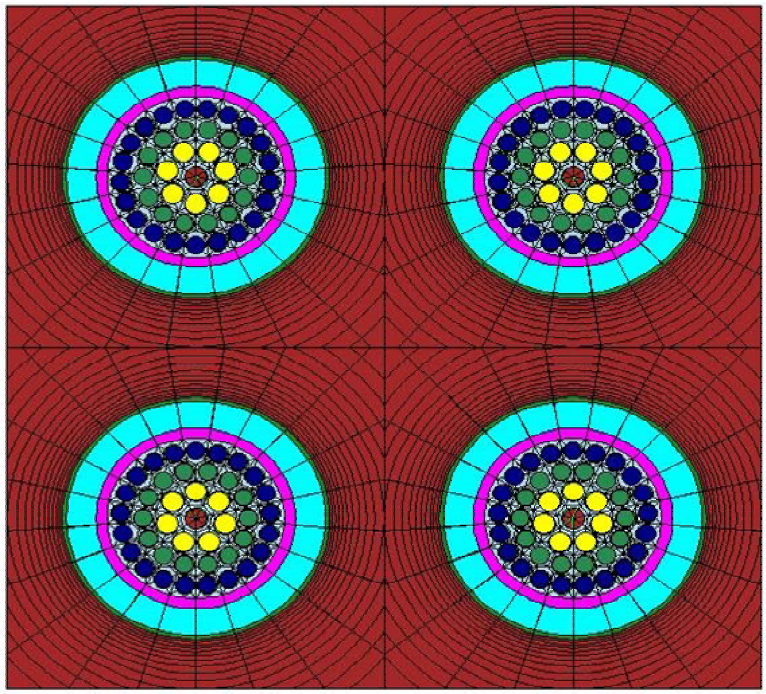

Figure 6 HELIOS 2x2 Lattice Physics Model

Table 5 Conditions Used for 2x2 HELIOS Analysis

Fuel Temp.	C	687
Coolant Temp.	C	300
Moderator Temp.	C	69
Coolant Density	g/cm^3	0.7209 (Cooled) .001 (Voided)
Coolant Purity	Wt% H2O	100
Moderator Purity	Wt% D2O	99.935
Moderator Poison	ppm	0

The following subsections will first provide results for various voiding scenarios of the 2x2 lattice and then a physics analysis will be provided of the checkerboard voided configuration.

II.B.1 2x2 Lattice Results

Several different burnup distributions were analyzed for the 2x2 configurations. In the first set of cases the burnup of all assemblies is the same (homogenous), with one case at zero burnup and another at an equilibrium burnup (12.3 Gwd/t). The second set of cases is for the more practical scenario in which two different fuel burnups are used. For all cases, both complete and partial "checkerboard" voiding configurations were considered.

Homogeneous Burnup Case: Zero Burnup, No Xenon

The first homogeneous case examines fresh fuel with no Xenon. As a basis of comparison, the same calculation was performed at CNSC [Serghuita, 2004b] using the same version of HELIOS (v1.8) and the same 47-group library, however, there were slight differences in the models (e.g. spatial discretization). The CNSC model [Serghita, 2004] is shown in Figure 7.

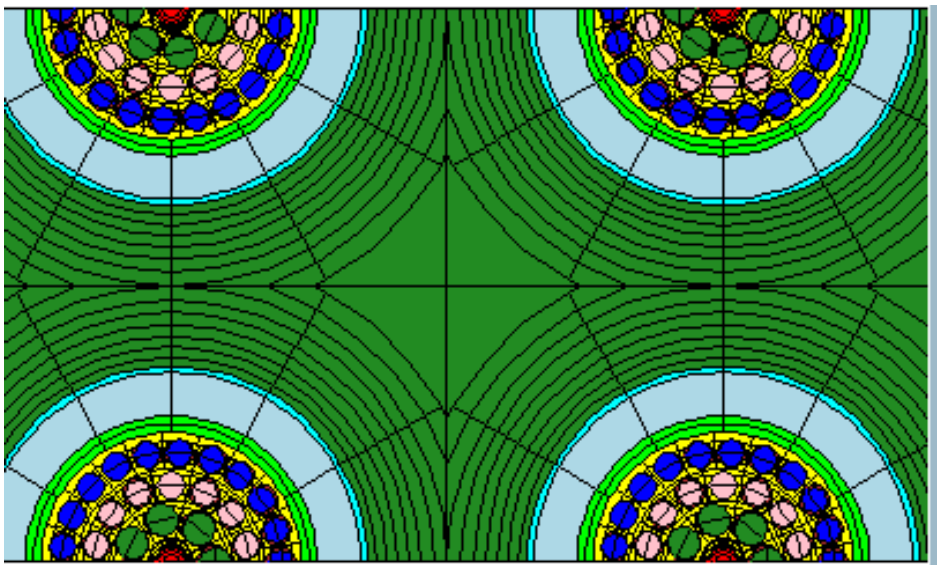

Figure 7 HELIOS 2x2 Model Used for CNSC Calculations

A comparison of the CNSC and Purdue calculations is shown in Table 6. The minor differences in the results can be attributed to small differences in the models and numerical discretization methods. As indicated both codes predict a negative CVR for the fully voided case and a positive CVR for the checkerboard voided case. A detailed physics analysis of the positive CVR in the checkerboard case will be provided in Section II.B.2.

Table 6 Comparison of Purdue and CNSC 2x2 HELIOS Results

	keff			CVR (mk)	
	Cooled	CB-Voided	Full-Voided	CB Voided	Full-Voided
Purdue Model	1.25378	1.26007	1.25260	+3.5	-2.1
CNSC Model	1.25356	1.25878	1.25052	+3.3	-1.9

Homogeneous Burnup Case: 12.3 Gwd/t Burnup, Eq. Xenon

The second homogeneous case used a fuel burnup of 12.3 Gwd/t at equilibrium Xe conditions. A PARCS 2x2 calculation was also performed in which the two group cross sections were generated from separate "zero current" single assembly HELIOS calculations. The use of "homogenized", zero current single assembly cross sections in PARCS is currently the standard procedure used in all LWR core calculations. The results are summarized in Table 7.

Table 7 Results for Homogeneous Burnup Case (12.3 Gwd/t, Eq. Xe, w/o ADFs)

	B.C	keff			CVR (mk)	
		Cooled	CB-Voided	Full-Voided	CB-Voided	Full-Voided
HELIOS (47-G)	**Periodic**	**1.03073**	**1.03571**	**1.02717**	**4.7**	**-3.4**
PARCS (2-G)	**Periodic**	**1.03080**	**1.03291**	**1.02699**	**2.0**	**-3.6**
HELIOS-PARCS (pcm)	**Periodic**	**-10**	**280**	**18**		

As indicated, the CVR for the fully voided case is again negative, where it is positive for the checkerboard voided case. A comparison of the HELIOS and PARCS/HELIOS result indicates that the k-eff of the fully cooled and fully voided configurations are in reasonably good agreement with a difference in both cases of less than 20pcm, and therefore the CVR for the fully voided case is also in reasonably good agreement. However, the PARCS/HELIOS result for the checkerboard voided case is significantly different than the HELIOS result. The primary source of discrepancy is the use of homogenized cross sections in PARCS, as will be shown in the next section.

Heterogeneous Burnup Case

A heterogenous burnup distribution is more realistic and the therefore the analysis was continued with a more practical burnup distribution for the 2x2 array as shown in Figure 8:

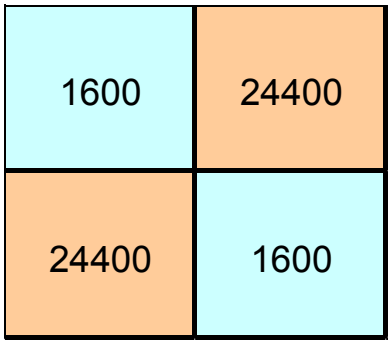

Figure 8 Burnup Distribution for 2x2 Heterogeneous Analysis

Two different checkerboard voiding configurations were used for this analysis. In the CB-1 case the low burnup fuel (1600 Mwd/t) was voided and the high burnup fuel (24400 Mwd/t) remained cooled, and in CB-2 the opposite case was analyzed in which the high burnup fuel was voided and low burnup fuel remain cooled. The results for these cases are shown in Table 8. Two different sets of PARCS calculations were performed, one without the use of Assembly Discontinuity Factors (ADFs) and the other with ADFs extracted from the single assembly calculation as the ratio of the surface and node average flux [Smith, 1980].

Table 8 Results for 2x2 Heterogeneous Burnup Case

		Cooled	CB1-Voided	CB2-Voided	Full-Voided	CB1-Voided	CB2-Voided	Full-Voided
HELIOS (47-G)	Periodic	1.03505	1.03719	1.04205	1.03140	+2.0	6.5	-3.4
PARCS w/o ADFs (2-G)	Periodic	1.03846	1.03715	1.04421	1.03544	-1.2	5.3	-2.8
HELIOS-PARCS (pcm)	Periodic	-320	213	-316	-364			

The first result worth noting is that HELIOS predicts a fully voided CVR of -3.4mk for the heterogeneous burnup case which is similar to the -3.4mk for the uniform burnup case. This is consistent since the average burnup of the heterogeneous case is similar to the uniform burnup case. The next result worth noting is that the CVR predicted for the two checkerboard voided cases are both positive, but the CVR for the CB2 case in which the low burnup fuel remains cooled is considerably more positive. It is then worth noting that there is a significant difference in the prediction of the k-effective between the PARCS/HELIOS and the HELIOS results for all the heterogeneous burnup cases. As was shown in the homogeneous burnup cases in Table 5, only the HELIOS and PARCS/HELIOS results for the checkerboard voided case were significantly different. However, in the heterogeneous case the k-effective results in all cases are noticeably different. It should be noted that the CVR predictions for the fully voided and the CB2 case are in reasonably good agreement because of a consistent bias in the k-effective of the cooled and voided configurations. However, the cancellation effect does not occur for the CB1 case and the CVR predicted by PARCS/HELIOS (-1.2mk) is of **opposite sign** than the HELIOS result (+2.0mk).

The principal source of error in the PARCS/HELIOS prediction of the k-effective and CVR for the heterogeneous burnup case is the use of HELIOS homogenized, single assembly cross sections in PARCS. This was demonstrated by using "color set" cross sections in PARCS in which the HELIOS cross sections were edited directly from the 2x2 assembly calculation instead of from the single assembly "zero current" calculations. As indicated in Table 9, the errors in all cases is considerably reduced, and the PARCS/HELIOS predictions of the CVR in both CB1 and CB2 cases are in reasonably good agreement with the HELIOS result.

Table 9 Results for 2x2 Heterogeneous Burnup Case: PARCS with HELIOS "Colorset" Cross Sections (w/o ADFs)

		keff				CVR (mk)		
	B.C	Cooled	CB1-Voided	CB2-Voided	Full-Voided	CB1-Voided	CB2-Voided	Full-Voided
PARCS (2-G) w/o ADFs	Periodic	1.03418	1.03628	1.04196	1.03053	2.0	7.2	-3.4
HELIOS (47-G)	Periodic	1.03505	1.03719	1.04205	1.03140	2.0	6.5	-3.4
HELIOS-PARCS (pcm	Periodic	87	91	9	87			

As will be discussed in section III, the use "color set" cross sections is not practical for core calculations. In LWR analysis, Assembly Discontinuity Factors are normally used to reduce the homogenization error. These factors are computed using in the zero current lattice calculation as the ratio of the surface flux to the node average flux. However, as shown in Table 10, the ADFs do not improve the accuracy of the heterogeneous 2x2 calculation.

Table 10 Results for 2x2 Heterogeneous Burnup Case

		Cooled	CB1-Voided	CB2-Voided	Full-Voided	CB1-Voided	CB2-Voided	Full-Voided
PARCS w/o ADFs (2-G)	Periodic	1.03846	1.03715	1.04421	1.03544	-1.2	5.3	-2.8
PARCS w/ ADFS (2-G)	Periodic	1.03825	1.03506	1.04521	1.03504	-3.0	6.4	-3.0
PARCS w/o ADFs - PARCS w/ ADFs (pcm)	Periodic	21	209	-100	40			

Alternately, the homogenization error can be reduced by the use of more energy groups in the core calculation, and therefore a sequence of multigroup PARCS calculations were performed and the results are shown in Table 11. As indicated in the Table, the error in the PARCS results generally reduces as the number of energy groups is increased, however, there remains some inconsistency in the results since the 8 group PARCS result is more accurate than the 47 group PARCS result.

Table 11 Comparison of PARCS Multigroup Calculations with HELIOS (w/o ADFs)

	B.C	keff				CVR (mk)		
		Cooled	CB1-Voided	CB2-Voided	Full-Voided	CB1-Voided	CB2-Voided	Full-Voided
PARCS (2-G)	Periodic	1.03846	1.03715	1.04421	1.03544	-1.2	5.3	-2.8
PARCS (4-G)	Periodic	1.03730	1.03545	1.04399	1.03409	-1.7	6.1	-3.0
PARCS (8-G)	Periodic	1.03739	1.03870	1.04291	1.03447	1.2	5.1	-2.7
PARCS (47-G)	Periodic	1.03690	1.03781	1.04269	1.03398	.8	5.4	-2.7
HELIOS (47-G)	Periodic	1.03505	1.03719	1.04205	1.03140	2.0	6.5	-3.4
HELIOS-PARCS2G (pcm)	Periodic	-341	4	-216	-404			
HELIOS-PARCS4G (pcm)	Periodic	-225	175	-194	-269			
HELIOS-PARCS8G (pcm)	Periodic	-234	-150	-86	-307			
HELIOS-PARCS47G (pcm)	Periodic	-185	-62	-64	-259			

II.B.2 Analysis of 2x2 Lattice Results

In order to better understand the partial voiding of the 2x2 lattice, detailed neutronics analysis was performed on homogeneous and heterogeneous 50% voided configurations. The heterogeneous voided case was simulated by the actual checkerboard voiding of alternate assemblies, and the homogeneous voided case was simulated by a uniform 50% reduction of the coolant density in all four channels. This analysis would provide a consistent comparison since the checkerboard voiding and 50% homogeneous density reduction represent an equivalent reduction in the amount of coolant in the 2x2 array. The changes in the neutron spectrum for the checkerboard, 50% homogeneous density reduction, and full voiding are shown in Figure 9

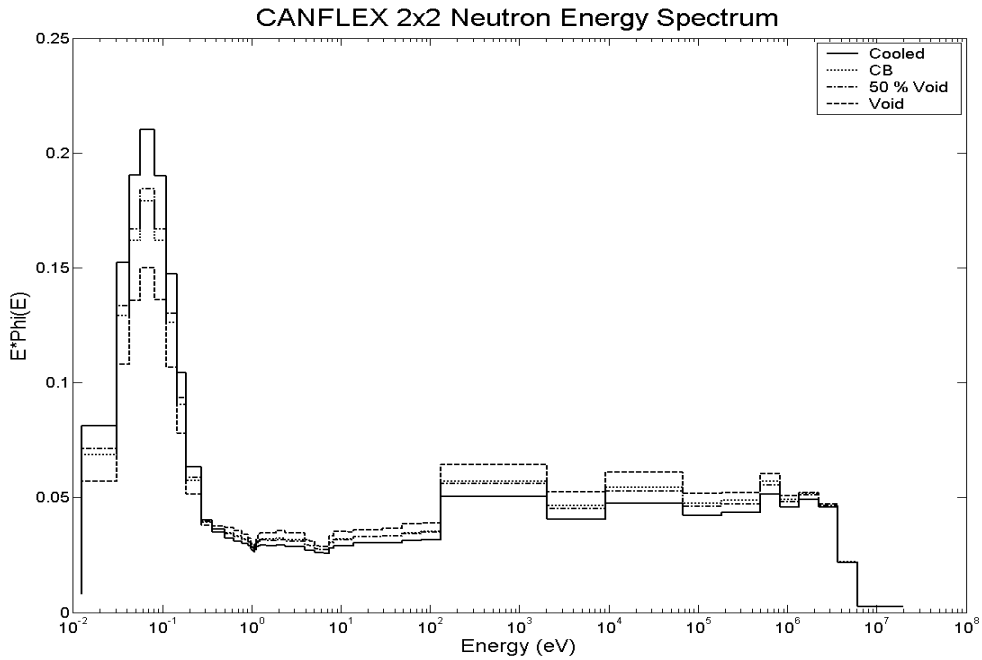

Fig. 9. Neutron Energy Spectrum for 2x2

As indicated, an overall neutron spectrum hardening occurs upon voiding as thermal neutrons are redistributed to higher energies due to the reduced moderation when the coolant density is reduced. There are slight differences in the spectra of the homogeneous and checkerboard voided cases. However, the most important physical effect is the spatial redistribution of the flux in the 2x2 array. In Figure 10, the spatial distribution of the flux is shown for three energy groups (1=fast, 2=epithermal, 3=thermal) for a traverse of the 2x2 problem from the cooled (CH1) to the voided (CH2) regions of the array. A comparison is made of the flux distribution in the Flooded (Cooled), Checkerboard Voided (CB), and Homogeneous 50% Voided (50% V) cases. As indicated, the voiding of neutrons in CH2 causes an increase in the neutron mean free path and a net leakage of epithermal neutrons from the voided region into the cooled region (Gr2 CB). (Note the "tilt" of the line Gr2 CB toward CH1 indicating a net current from the voided towards the flooded channel.) These neutrons are then moderated in the cooled region which results in a net leakage of thermal neutrons from the cooled region into the voided region (Gr3 CB). (Note the "tilt" of the line Gr3 CB toward CH2 indicating a net current from the cooled towards the voided channel). This is a "spatial self-shielding" effect which makes it possible for more fast neutrons to slow down to thermal without being absorbed, thereby increasing the resonance escape probability in the checkerboard voided case.

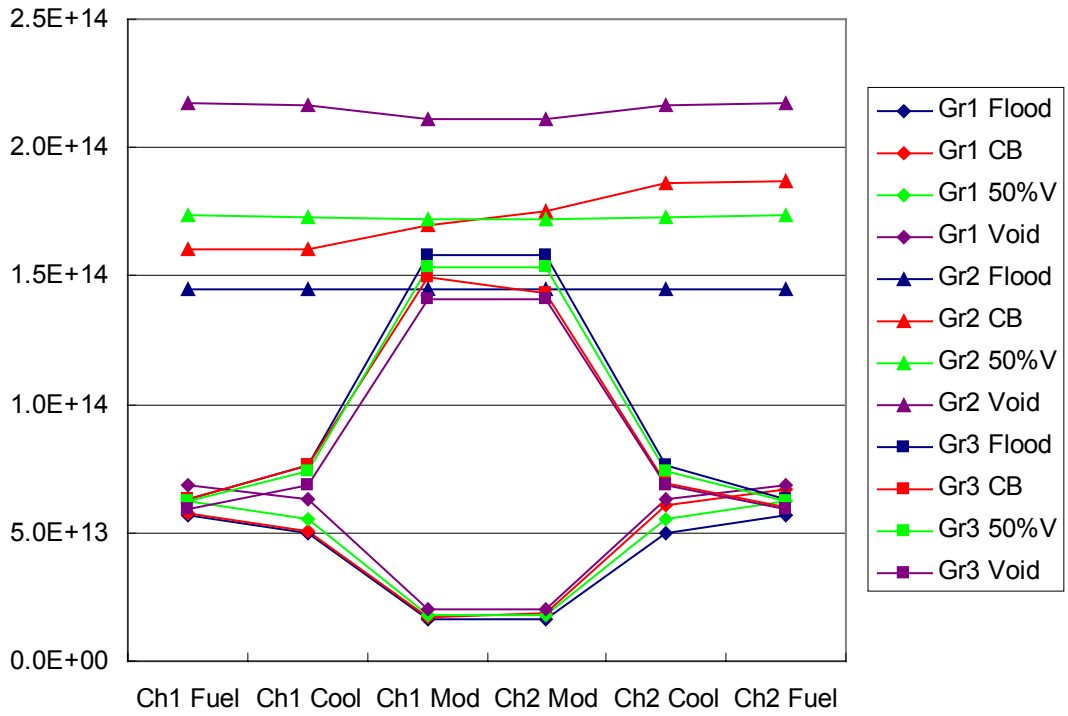

Figure 10 Spatial Distribution of Fluxes in 2x2 Channels

A "four factor" analysis was performed on the 2x2 assembly case and the results are summarized in Table 12. As indicated, the resonance escape probability for the checkerboard case is about 6.6 mk less negative than for the homogeneous voided case, which accounts for most of the difference in the CVR for the homogeneous and checkerboard cases, -2.5 mk vrs +3.5mk, respectively.

Table 12 Comparison of Four Factors for Checkerboard and Homogeneous Voided States

	50% Homogeneous Void	Checkerboard	Fully Voided
$\Delta\eta$	-1.8	-3.1	-5.2
Δf	18.7	20.7	39.9
$\Delta\varepsilon$	15.4	14.6	35.7
Δp_E	**-33.2**	**-26.6**	-68.5
Δp_F	-1.7	-2.0	-4.0
Sum	**-2.5**	**+3.5**	-2.1

II.C Mini-Core Analysis

The single assembly and 2x2 assembly analysis were then extended to 3-dimensional "mini-core" models of the CANDU-6 and ACR using PARCS with HELIOS cross sections. Part of the motivation for this sequence of calculations was the availability of published results from other researchers who analyzed the voiding of a sub-region of the CANDU-6 reactor [Rahnema, 2000], [Sarsour, 2004].

CANDU-6 4x3 Mini-Core Model

Figure 12 illustrates the CANDU-6 subregion model which consists of a region of four by three fuel channels from the center of the CANDU-6 reactor. Each channel contains six fuel assemblies and represents half of the 12 assemblies per channel in the reactor. Two burnup cases were examined, a uniform burnup distribution of 4000 Mwd/t and a distributed burnup case as shown in Table 13. The boundary conditions used to evaluate the model are reflective along the X-Y plane and zero neutron flux at Z = 0 and reflective at Z = 6. The model was constructed without reactivity control devices. The cross-sections for each assembly were generated using HELIOS v1.7.

.

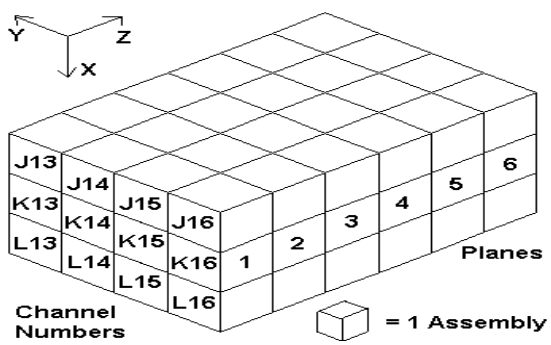

Fig. 11 CANDU-6 4x3 Subregion Model

Table 13 Burnup Distribution for 4x3 Heterogeneous Model

Bundle Channel	1	2	3	4	5	6
J-13	8077.59	9659.54	9754.64	8339.32	6549.57	7048.91
J-14	445.99	1046.64	1465.36	1672.34	1607.55	1741.21
J-15	8207.37	9108.32	8737.19	7077.67	5223.97	5630.14
J-16	1267.22	2965.31	4086.27	4632.18	4846.53	5263.38
K-13	1191.33	2757.16	3755.53	4165.82	4048.46	4374.86
K-14	7497.5	7894.16	7122.33	5150.62	3146.09	3393.34
K-15	192.28	448.5	630	721.34	701.61	759.05
K-16	7126.71	7793.59	7302.99	5630.17	4050.7	4394.62
L-13	6787.47	6469.88	5107.65	2652.13	622.08	673.76
L-14	577.08	1349.57	1874.15	2114.86	2020.63	2186.04
L-15	8505.58	9641.32	9392.78	7753.21	5783.44	6206.79
L-16	796.12	1878.76	2632.72	3022.98	3015.76	3265.46

Voiding patterns evaluated included a fully voided pattern, in which all assemblies are voided of the coolant, and a checker-board (CB-1) voiding pattern in which every other assembly is voided of the coolant. The results for the CANDU-6 model are shown in Tables 14 and 15, and compared with published CANDU-6 sub-region voiding results [Rahnema, 2000], [Sarsour, 2002].

TABLE 14 CANDU-6 Coolant Voiding Uniform Burnup (Uniform 4000MWd/TU)

CODE	Cooled k-eff	CB Void k-eff	Full Void k-eff	CB CVR [mk]	Full Void CVR [mk]
PARCS (2-Groups)	1.03458	1.04372	1.05318	8.46	17.1
MCNP [Rahnema, 2000]	1.03496	1.04303	-	7.48	-

Table 15 CANDU-6 Coolant Voiding Results Distributed Burnup

CODE	Cooled k-eff	CB Void k-eff	Full Void k-eff	CB CVR [mk]	Full Void CVR [mk]
PARCS (2-Groups)	1.02967	1.03858	1.04856	8.3	17.5
NESTLE [Sarsour, 2002]	1.03254	1.04112	1.04955	8.0	15.7
MCNP [Rahnema, 2000]	1.03001	1.04539	1.03817	7.6	14.3

The CANDU-6 results in both Tables 14 and 15 indicate that the HELIOS/PARCS results are in reasonable agreement with the coolant void predictions from NESTLE and MCNP.

ACR 4x4 Mini-Core Model

Similarly, an ACR-700 PARCS model was created using PARCS/HELIOS. Due to the differences in the number of channels in the CANDU-6 and ACR-700 reactors, a four by four model was used for the ACR-700 as shown in Figure 13. Cross sections were generated with HELIOS v1.7 and PARCS calculations were performed using the two group ANM kernel. The ACR-700 model was evaluated using a bundled average distribution provided by CNSC [Serghuita, 2004c] and at a uniform burnup of 12300 MWd/TU which corresponds to approximately the predicted mid-cycle burnup of a ACR-700 fuel assembly.

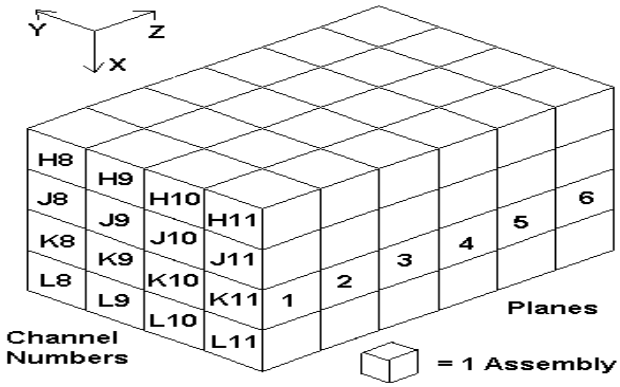

Plane 1

1600	24400	1600	24400
24400	1600	24400	1600
1600	24400	1600	24400
24400	1600	24400	1600

Plane 2

4000	24400	3900	24400
24400	4000	24400	3900
3900	24400	4000	24400
24400	3900	24400	4000

Plane 3

6900	23300	6800	23300
23300	6900	23300	6800
6800	23300	6900	23300
23300	6800	23300	6900

Plane 4

9600	21700	9600	21700
21700	9600	21700	9600
9600	21700	9600	21700
21700	9600	21700	9600

Plane 5

12400	19600	12300	19600
19600	12400	19600	12300
12300	19600	12400	19600
19600	12300	19600	12400

Plane 6

14900	17300	14800	17300
17300	14800	17300	14800
14800	17300	14800	17300
17300	17800	17300	14900

Figure 13 ACR-700 Mini-Core Model and Burnup Distribution

In the ACR-700 model, the CB-1 voiding pattern corresponds to the voiding of the low burnup channels. A second checker-board voiding pattern (CB-2) was also evaluated in which the high burnup fuel channels were voided. The ACR model was also constructed without representing reactivity control devices. The results for the uniform and distributed burnup cases are summarized in Tables 16 and 17, for the full coolant voiding and for the checkerboard voiding, respectively.

TABLE 16 ACR-700 Full Coolant Voiding

Case	Cooled k-eff	Full Void k-eff	Full Void CVR [mk]
Uniform 1600 [MWd/TU]	1.18282	1.17898	-2.8
Uniform 12300 [MWd/TU]	1.02442	1.01774	-6.4
Bundle Average Distribution	1.01816	1.00941	-8.5

TABLE 17 ACR-700 Checkerboard (CB) Coolant Voiding

Case	CB-1 k-eff	CB-2 k-eff	CB-1 CVR [mk]	CB-2 CVR [mk]
Uniform 1600 [MWd/TU]	1.18445	NA	1.5	NA
Uniform 12300 [MWd/TU]	1.02483	NA	0.4	NA
Disbributed Burnup	1.01305	1.02160	-5.0	3.3

The results indicate that under full voiding conditions both the uniform and distributed burnup arrangements lead to a negative CVR in the ACR-700. However, the uniform cases indicate a positive CVR for checker-board pattern 1 (CB-1) voiding and the distributed burnup cases indicate a positive CVR for the checker-board pattern 2 (CB-2) voiding.

II.D Full Core Calculations

The final sequence of calculations was to perform a preliminary full core analysis of the ACR with PARCS using HELIOS cross sections. Several cases were examined and the results of each will be briefly reviewed in this section.

II.D.1 Uniform Core Loading (2-D)

In order to isolate the effect of core leakage on the CVR, The first case was to exam the most simplified core configuration with a single fuel type having a burnup of 1600 Mwd/t (Type=3) and a reflector of two assembly thickness (Types 1,2). The core configuration is show in Figure 14.

					1	1	1	1	1	1	1	1	1	1	1	1						
				1	1	2	2	2	2	2	2	2	2	2	2	1	1					
			1	1	2	3	3	3	3	3	3	3	3	3	3	2	1	1				
		1	1	2	3	3	3	3	3	3	3	3	3	3	3	3	2	1	1			
	1	1	2	3	3	3	3	3	3	3	3	3	3	3	3	3	3	2	1	1		
1	1	2	3	3	3	3	3	3	3	3	3	3	3	3	3	3	3	3	2	1	1	
1	2	3	3	3	3	3	3	3	3	3	3	3	3	3	3	3	3	3	3	2	1	
1	2	3	3	3	3	3	3	3	3	3	3	3	3	3	3	3	3	3	3	2	1	
1	2	3	3	3	3	3	3	3	3	3	3	3	3	3	3	3	3	3	3	2	1	
1	2	3	3	3	3	3	3	3	3	3	3	3	3	3	3	3	3	3	3	2	1	
1	2	3	3	3	3	3	3	3	3	3	3	3	3	3	3	3	3	3	3	2	1	
1	2	3	3	3	3	3	3	3	3	3	3	3	3	3	3	3	3	3	3	2	1	
1	2	3	3	3	3	3	3	3	3	3	3	3	3	3	3	3	3	3	3	2	1	
1	2	3	3	3	3	3	3	3	3	3	3	3	3	3	3	3	3	3	3	2	1	
1	2	3	3	3	3	3	3	3	3	3	3	3	3	3	3	3	3	3	3	2	1	
1	2	3	3	3	3	3	3	3	3	3	3	3	3	3	3	3	3	3	3	2	1	
1	2	3	3	3	3	3	3	3	3	3	3	3	3	3	3	3	3	3	3	2	1	
1	1	2	3	3	3	3	3	3	3	3	3	3	3	3	3	3	3	3	2	1	1	
	1	1	2	3	3	3	3	3	3	3	3	3	3	3	3	3	3	2	1	1		
		1	1	2	3	3	3	3	3	3	3	3	3	3	3	3	2	1	1			
			1	1	2	3	3	3	3	3	3	3	3	3	3	2	1	1				
				1	1	2	2	2	2	2	2	2	2	2	2	1	1					
					1	1	1	1	1	1	1	1	1	1	1	1						

Figure 14 ACR Core Layout for Preliminary Full Core Calculation

Reflector cross sections were generated using a multi-assembly HELIOS model as shown below in Figure 15. The reflector cross sections for the regions adjacent to the fueled region were edited as reflector types 1 and 2, respectively.

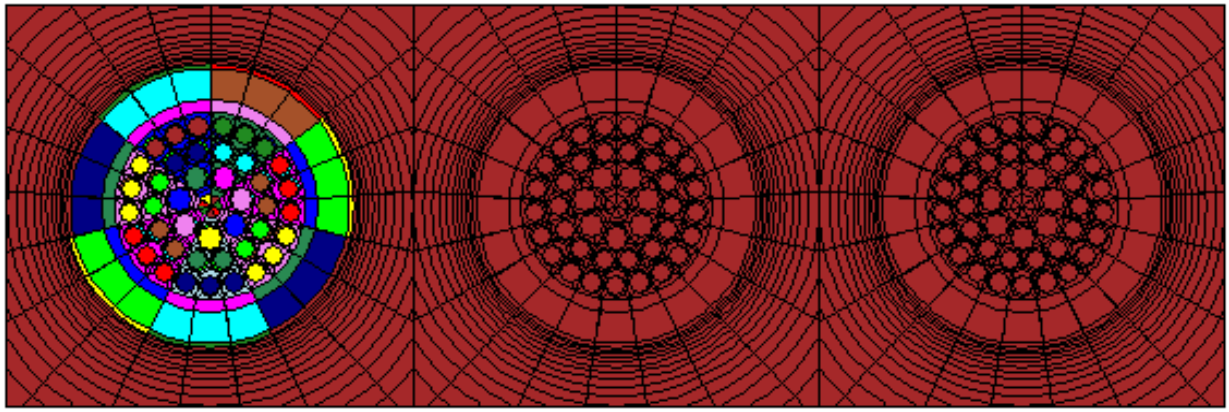

Figure 15 HELIOS Model for Reflector Cross Sections

The PARCS calculation was performed using 2 energy groups with zero incoming current boundary conditions at the surface of the outermost reflector. The results for the uniform core model calculation are shown in Table 18. By comparing the k-effective of the PARCS cooled full core calculation (1.17202) with the k-effective of a PARCS cooled 2x2 "zero current" calculation (1.19005), the leakage reactivity of the 2-D core can be estimated to be about 1.8%k. A comparison of the CVR of the PARCS full core and PARCS 2x2 indicates that the 2-D core leakage provides a negative reactivity effect of about 1.8 mk for the fully voided core and about 1.0 mk for the checkerboard voided core.

Table 18 Results for Uniform 2-D Full Core Calculation

	B.C.	k_{eff}			CVR (mk)	
		Cooled	CB-Voided	Full-Voided	CB-Voided	Full-Voided
PARCS Full Core (2-D) (2-G)	Zero Incoming Current	1.17202	1.17478	1.16911	2.0	-2.1
PARCS 2x2 (2-G)	Periodic	1.19005	1.19425	1.18963	3.0	-0.3
HELIOS 2x2 (47-G)	Periodic	1.19004	1.19684	1.18992	4.8	-0.1

The basis for the negative reactivity effect of the core leakage on the CVR is apparent by comparing the core flux distributions before and after voiding. As indicated in Figure 15 below, upon core voiding there is a significant increase in the thermal and fast (not shown) flux distribution at the core periphery. The percent change is summarized in Figure 17.

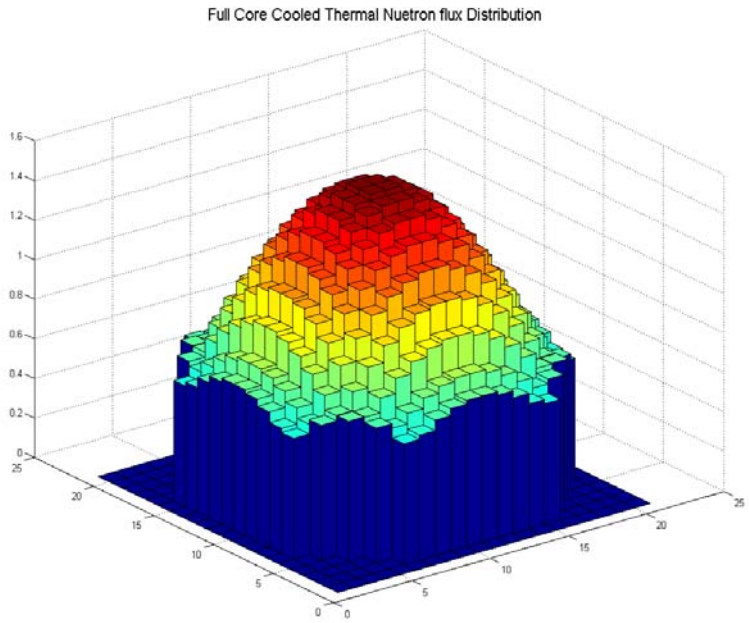

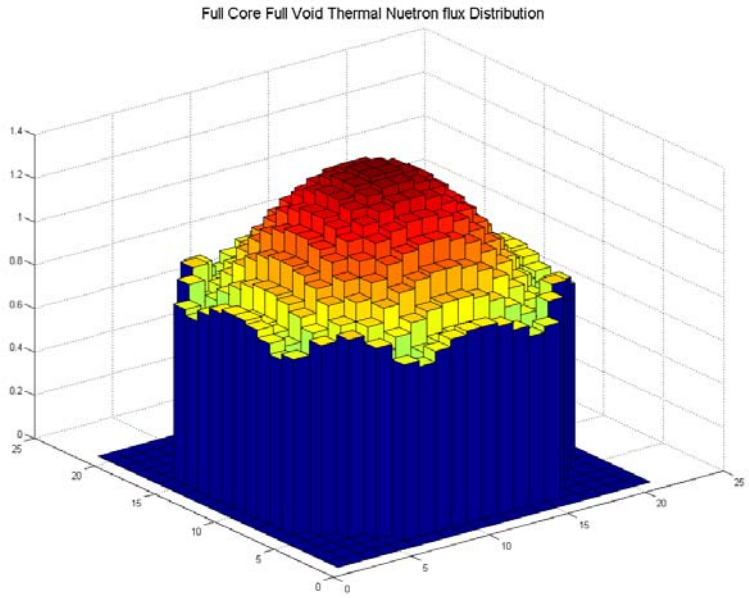

Figure 16 Thermal Flux Distributions Before and After Core Voiding

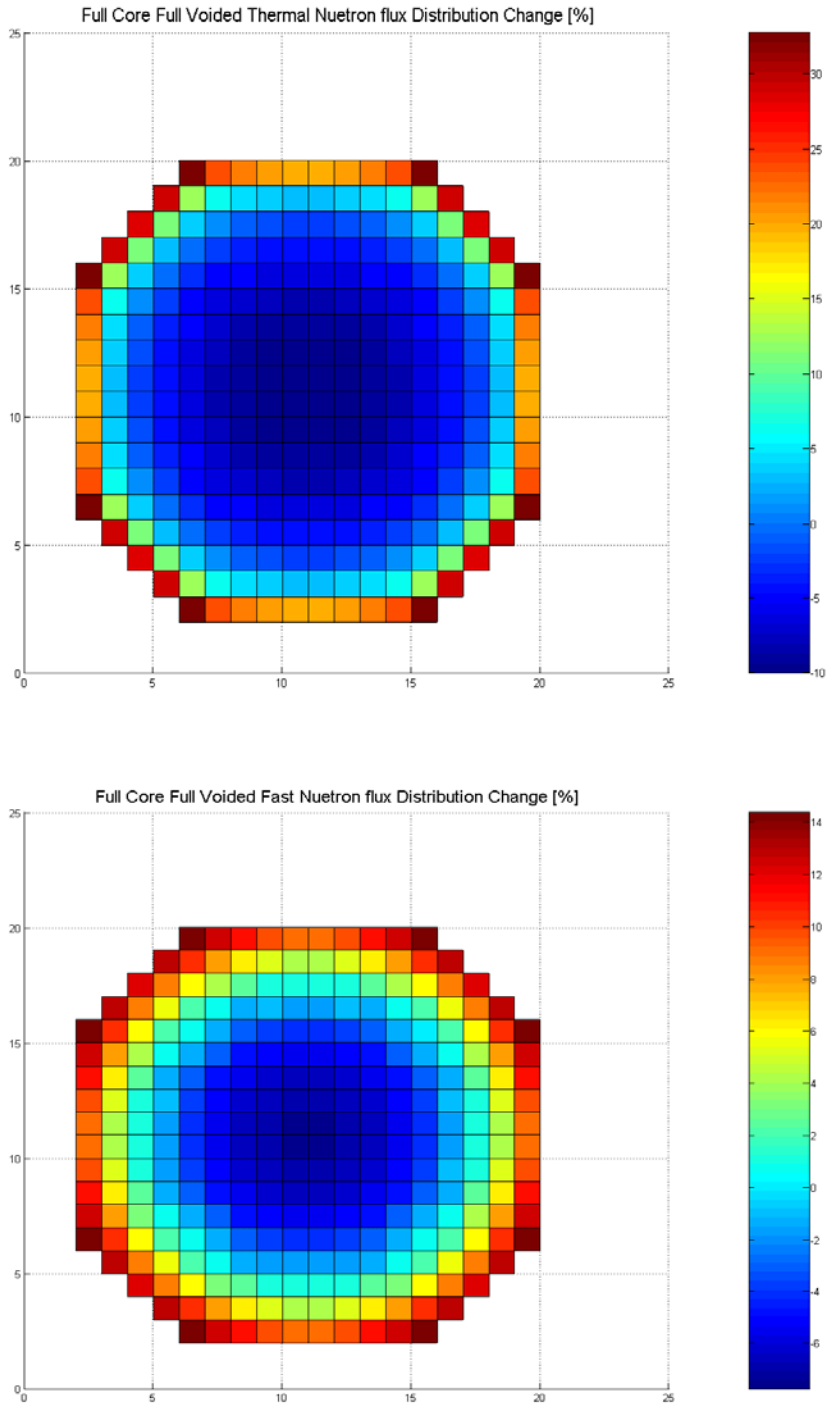

Figure 17 Change in Thermal and Fast Flux Distributions for Uniform Core

As was indicated in Table 17, the negative reactivity contribution of the radial core leakage to the CVR is about 0.8 mk smaller for the checkerboard voided case. This is because of the smaller flux increase at the periphery as shown in Figure 18 for the Checkerboard Voided core.

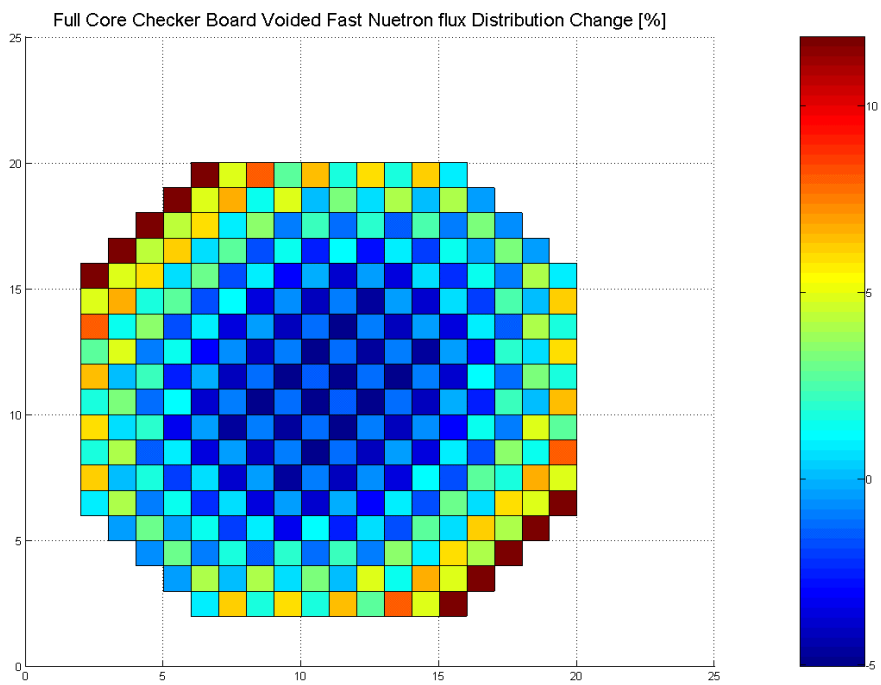

Figure 18 Change in Fast Flux upon Checkerboard Voiding

In order to assess the validity of the core reflector model, a second calculation was performed in which an additional row of assemblies was added to the HELIOS reflector cross section model, as well as to the PARCS full core model. As indicated, adding a row of reflectors reduces the negative reactivity effect of the core leakage on the CVR. The actual ACR-700 core reflector is 52 cm thick which is between the two cases shown in the Table 19.

Table 19 Summary of Results for Analysis of the Reflector Core Model

	Radial B.C.	Axial B.C.	keff			CVR (mk)	
			Cooled	CB-Voided	Full-Voided	CB-Voided	Full-Voided
PARCSFull Core (2-G) (Refl = 44cm)	Zero Incoming Current	Reflective	1.17202	1.17478	1.16911	2.0	-2.1
PARCSFull Core (2-G) (Refl = 66cm)	Zero Incoming Current	Reflective	1.17576	1.17964	1.17570	2.8	0.0

II.D.2 Uniform Core Loading (3-D)

A full 3D PARCS calculation was then performed to assess the impact of axial core leakage. No reflector was placed on the axial boundary because of the presence of the refueling machine. As indicated in the Table 20, the axial core leakage accounts for an additional 0.6%k in the k-effective. Comparing the results to the PARCS 2x2 calculation indicates that the total negative leakage effect on the CVR for the uniform core is about -3.7mk.

Table 20 Summary of Results for 3D PARCS Core Calculation

Refl = 44cm	Radial B.C.	Axial B.C.	keff			CVR (mk)	
			Cooled	CB-Voided	Full-Voided	CB-Voided	Full-Voided
PARCSFull Core (2-G) (3-D)	Zero Incoming Current	ZeroIncoming Current	1.16551	1.16715	1.16012	1.2	-4.0
PARCSFull Core (2-G) (2-D)	Zero Incoming Current	Reflective	1.17202	1.17478	1.16911	2.0	-2.1
PARCS 2x2 (2-G)	Periodic		1.19005	1.19425	1.18963	3.0	-0.3

II.D.3 Heterogeneous Core Loading (3-D)

The more realistic heterogeneous core loading was then analyzed as shown in Figure 18. Fuel Types 3 and 4 were used with burnups of 1600 Mwd/t and 24400 Mwd/t, respectively. The alternating arrangement of fuel types 3 and 4 was also used in the axial direction to simulate a heterogeneous 3-D distribution. All cross sections were generated using 2x2 HELIOS assembly models to minimize the homogenization errors. No reflector was used in the axial direction.

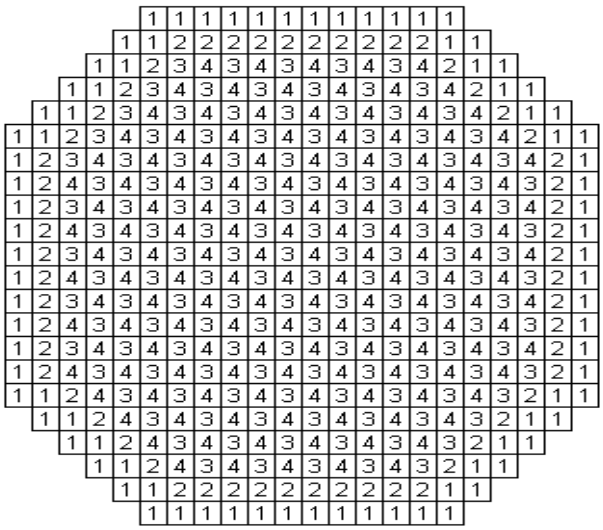

Figure 19 Heterogeneous Core Loading

Two checkerboard voiding configurations were examined, one in which the low burnup fuel was voided (CB-1) and the second in which the high burnup fuel was voided (CB-2). The results are shown in the Table 21 below. In all cases a 44 cm reflector was used in the radial direction and no reflector was used in the axial direction.

Table 21 PARCS Results for Full Core Checkerboad Voided Configurations

	Radial B.C.	Axial B.C.	keff				CVR (mk)		
			Cooled	CB-1 Voided	CB-2 Voided	Full-Voided	CB-1 Voided	CB-2 Voided	Full-Voided
2-D	Zero Incoming Current	Reflective	1.01911	1.02039	1.02575	1.01389	1.2	6.3	-5.1
3-D	Zero Incoming Current	Zero Incoming Current	1.01335	1.01361	1.01909	1.00598	0.3	5.6	-7.2

The 3-D full core voided PARCS CVR result in Table 21 (-7.2mk) agrees well with the AECL result (-7.0mk) reported at the PIRT expert panel meeting in Washington DC on October 30 and 31, 2003 [AECL, 2003b].

The PARCS results were also compared to a CNSC MCNP full core result [Serghurita, 2004d]. Their model used a checkerboard arrangement with two fuel burnups (0 and 20076 Mwd/t), which differed slightly from the arrangement used in the PARCS model. Also, the checkerboard voiding strategy was slightly different than that used in PARCS. Nonetheless, the full core and checkerboard voided CVR predicted by the CNSC MCNP model of -6.5 mk and +3.6 mk [Serguita, 2004d] were similar to the PARCS results in Table 21.

III. Modifications to the PARCS Code Required for ACR Analysis

The modifications to the PARCS code required for ACR analysis can be classified into two general categories. The first type are the obvious coding changes necessary to capture the basic functionality of the ACR in PARCS. The second type are the methods modifications that have become apparent based on the analysis summarized in section II. The following section will first summarize the coding changes, and section III.B will then outline the methods modifications.

III.A Coding Modifications to the PARCS Code

1. Core Geometry Modeling. The ACR is a **horizontal geometry** with irregular **"notches"** at either end of the core. This will require some modifications to the PARCS coding, as well as Input Cards / Output Edits / User Manual.

2. Reactivity control mechanisms The ACR has several specialized reactivity control mechanism that will require some modifications to PARCS. Some of these devices are inserted perpendicular to the reactor central axis whereas PARCS currently only treats LWR type reactivity control which are inserted axially into the core. Specifically, special treatment will be required for:

i. Zone Control Units (ZCU)
ii. Mechanical Control Absorber Units (MCAs)
iii. Shut Off Units (SU) (SDS1)
iv. Liquid Injection Shutdown Units (SDS2)
v. Modeling methods for 3D devices
    1. New input processing of control rod locations
    2. Horizontal insertion w/ pre-tabulated insertion rate
    3. Explicit modeling of liquid flow into vessel

3. Cross section model:

The objective of the cross section model in PARCS is to provide a sufficiently accurate model for coupling the neutron cross sections and other lattice nuclear data to the thermal-hydraulic and mechanical feedback in the core for both steady-state and transient conditions. The accuracy of the cross section model should be such that any errors introduced by neglecting a physical phenomena should be small in comparison to errors introduced by other methods approximations. In order to meet this criteria for the ACR some modifications to the PARCS cross section model will be required to describe unique features of the ACR.

i. **Additional feedback variables**. Currently PARCS treats a combined coolant / moderator as a single variable. In the ACR, the coolant and moderator are separate, and therefore an additional variable will have to be added to the PMAXS file. Depending on the level of sophistication required, it may also be necessary to add the purity of the coolant and moderator as a dimension on the cross section.

ii. **3-D Cross Section Modeling.** In order to treat the horizontal reactivity devices, it will be necessary to modify the cross section model in PARCS.

iii. **Kinetics Data.** For kinetics analysis, it is not yet clear if explicit modeling of additional delayed neutron groups or photo-neutron data would be required. If so, these would be minor additions to PMAXS.

4. TRACE Mapping. Modifications to the TDMR/PARCS will be required to accommodate unique features of the ACR channels in TRACE.

5. Other Modifications. The modifications listed above should be sufficient to perform core safety analysis with TRACE/PARCS. However, if PARCS is required to have the same functionality as the AECL core simulator RFSP [AECL, 2003b], then a few additional modifications would be required. These would include:

i. Modeling of the Reactor Regulating System (RRS) logic for controlling the ZCU.
ii. Modeling of the In-Core Detector System
ii. Modeling on-line refueling logic would be required for depletion analysis.

III.B PARCS Methods Improvements for ACR Analysis

The methods approximations used in the PARCS code can be categorized into four general areas:

1. Homogenization / Dehomogenization
2. Number of Energy Groups
3. Transport Approximation
4. Spatial Discretization

Based on the analysis in section II, it appears that only the first of these four approximations, homogenization / dehomogenization, will require significant modification for the application of PARCS to the ACR-700.

III.B.1 Homogenization / Dehomogenization

The homogenization / dehomogenization approximation in neutronics is a direct result of the traditional "two step" process used to solve the Boltzmann transport equation for reactor core simulation [Smith, 1980]. In this process, the first step is to use an integral transport lattice code to solve for the fuel assembly cross sections or "coefficients" of the Boltzmann equation, and the second step is to solve the Boltzmann equation itself using a global core simulator such as PARCS. Homogenization refers to the "smearing" of the spatial details of assembly geometry and composition and collapsing of the energy spectra into a single set of "homogenized" cross sections which can be used in the core calculation. Since the ultimate goal of core simulation is often the prediction of fuel pin powers, a "dehomogenization" is necessary after the core power calculation in which the global flux shapes are combined with the details of the heterogeneous assembly calculation to predict the pin-wise flux and power distribution. Homogenization and dehomogenization methods have been successfully applied in the Light Water Reactor industry for the last several years. This section will briefly review some of the issues that should be addressed if these methods are to be accurately applied to the ACR.

Homogenization

It was noted in Section II.B that the traditional use of homogenized "zero current" cross sections in PARCS can lead to significant errors in the prediction of the coolant void reactivity in the checkerboard voiding case. In the 2x2 example shown in Table 6, the CVR predicted by PARCS using two energy group HELIOS zero current single assembly cross sections was significantly different from the HELIOS 2x2 calculation, differing in magnitude by more than 5 mk and being opposite in sign. In section II.B (Table 8), it was shown that the traditional method used in LWRs to employ Assembly Discontinuity Factors (ADFs) was not adequate for the much more heterogeneous ACR lattice. It was also noted in section II.B that the error could be reduced somewhat

by using more energy groups in the core simulator. However, even using more than 8 energy groups in PARCS, some homogenization errors persisted both for internodal leakage between channels as well as for leakage from peripheral channels to the adjacent reflector regions. Homogenization was cited in the nuclear analysis PIRT analysis as having the largest discrepancy between importance and knowledge level relates to spatial homogenization of cross sections for use in core simulations.

Therefore it is recommended that homogenization techniques be one of the primary focuses of methods improvements in PARCS. It was shown in section II.B (Table 9) that the direct use of "color set" cross sections in PARCS provided acceptable results. In this approach, instead of using the "zero current" assembly cross sections, the single assembly cross sections are extracted from the 2x2 HELIOS calculation which accurately depicts the ambient boundary conditions. However, the color set technique is not practical because of the numerous combinations of 2x2 calculations that would be necessary to simulate all the possible combinations present in an equilibrium core environment.

Several researchers have proposed possible solution to the homogenization problem for LWR analysis. [Smith, 1995] and [Clarno, 2004] have proposed the introduction of dynamic, "on-line" methods that can be used to correct for homogenization errors during the course of the solution convergence. Clarno suggested the use of an albedo boundary condition for the lattice calculation that can be used in the core calculation as a "feedback" parameter similar to the current temperature / density feedback for thermal-hydraulics calculations. It is very likely that such a method, in combination with more energy groups, should provide an acceptable modification to PARCS for the ACR. The improved homogenization methods can be validated with a combination of numerical (e.g. Monte Carlo and Integral Transport benchmarks) and experimental benchmarks (e.g. ZED-2). The power distributions from the ZED-2 experiments will be particularly important since they will provide measurements within the fuel bundle and measurements at a simulated core-reflector interface.

Dehomogenization

It was noted in the PIRT nuclear analysis that the calculation of the fuel pin powers for LOCA analysis is one of the most important issues to resolve. In LWR analysis, modern flux reconstruction techniques such as those currently used in PARCS, have been able to predict successfully fuel pin powers to within 1% of measured data [Joo, 2002], [Grimm, 1996]. These same techniques may not be directly applicable to the ACR because of its more complex geometry and heterogeneous compositions (e.g. central Dysprosium pin and multiple fuel enrichments). Therefore some modification will be required to the current PARCS pin power reconstruction method.

A background investigation was performed on the state-of-the-art in flux reconstruction methods for CANDU reactors. A method was developed and tested by the Koreans in 2000 [Lee, 2000]. In this method, a coarse mesh finite difference code similar to PARCS is used in conjunction with a lattice physics code similar to HELIOS to reconstruct the few group fluxes. The homogeneous intranodal distributions are computed using polynomial flux shapes constrained to satisfy the nodal information approximated from the node average fluxes in the core simulator. The group fluxes of the individual fuel pins in a heterogeneous fuel bundle are determined using the "form functions" obtained from the single assembly lattice calculations and the reconstructed homogeneous intranodal flux distribution. The pin powers are then determined using the reconstructed pin fluxes. The accuracy of the reconstructed scheme was estimated using higher order numerical benchmark calculations for partial core representations of the CANDU reactor. Their results indicate that the reconstruction schemes are reasonably accurate, yielding maximum pin power errors of less than 3%. They note that the primary contribution to the error is from the errors in the node average fluxes obtained from the coarse mesh calculation.

This work will provide a very useful starting point for modifying the current homogenization scheme in PARCS to accommodate the ACR. However, the stronger heterogeneities in the ACR compared to the CANDU-6 may require some additional considerations.

III.B.2 Other Methods Modifications

In previous PARCS development efforts related to the LWR MOX project, modifications were made to PARCS to treat more energy groups, higher order spatial discretization schemes, and an SP3 transport approximation. All of these modifications will be directly applicable to the ACR and therefore no additional modifications will be needed in the areas of additional energy groups, spatial discretization, or transport approximation. However, it will be important to perform sensitivity studies using these methods for the ACR and to compare solutions to higher order results (e.g. Monte Carlo), as well as to experimental data.

IV. References

[AECL, 2003a] Atomic Energy of Canada Limited. (2003). ACR-700 Technical description. (10810-01371-TED-001Revision 0). Ontario, Canada: AECL

[AECL, 2003b] Safety Aspects of the ACR Design, page 27. PIRT meeting in Washington DC on October 30 and 31, 2003.

[Clarno, 2004] K. Clarno and M. Adams, "Capturing the Effects of Unlike Neighbors in Single-Assembly Calculations," submitted for publication, Nuclear Science and Engineering, March, 2004.

[Diamond, 2004] Phenomena Identification and Ranking Technique Applied to the ACR-700, Report to the U.S. NRC, April, 2004.

[Downar, 2002] T. J. Downar, et. al., "PARCS: Purdue Advanced Reactor Core Simulator." PHYSOR 2002. Seoul, Korea, Oct. 7-10 (2002).

[Grimm, 1996] P. Grimm, M Aboudy, A. Galperin, M Segev, "A Test of Main Stream Pin Power Reconstruction Methods," Nuclear Science and Engineering, 122, 395-406 (1996).

[Joo, 2002] H. Joo, Q. Zee, T. Downar, D. Ebert, "Consistent Analytic Pin Power Reconstruction Method for Static and Transient Reactor Safety Analysis," ANS Mathematics and Computation Meeting, Madrid, Spain, 2002.

[Lee, 2000] H.S. Lee, et. al, "A Pin Power Reconstruction Method for CANDU Reactor Cores Based on Coarse Mesh Finite Difference Methods," Nuclear Technology, Vol. 130, April, 2000.

[Ovanes, 2002] "Reactor Physics Innovations in the ACR-700 Design for Next Generation CANDU," 23rd CNS Annual Conference, June 3-5, 2002.

[Rahnema, 2000] F. Rahnema, S. Mosher, M. Pitts, P. Akhtar and D. Serghiuta, "MCNP Simulation of Void Reactivity in a Simplified CANDU Core Sub-Region", Proceedings of the International Conference Monte-Carlo-2000, Lisbon (2000).

[Sarsour, 2002] H.N. Sarsour, F. Rahnema, S. Mosher, P.J.Turinsky, D. Serghiuta, G. Marleau, and T. Courau, "HELIOS/DRAGON/NESTLE Codes' Simulation of Void Reactivity in a CANDU Core," 23rd Nuclear Simulation Symposium, Ottawa, November 3 - 5, 2002

[Smith, 1994] K. S. Smith, "Practical and Efficient Iterative Method for LWR Fuel Assembly Homogenization," Trans. Am. Nucl. Sci., 71, 238-241 (1994).

[Smith, 1980] K. Smith, "Spatial Homogenization Methods for Light Water Reactor Analysis," PhD Thesis, Massachusetts Institute of Technology, Cambridge, MA, June, 1980.

[Serghuita, 2004a] Private Communication, February, 2004.

[Serghuita, 2004b] Private Communication, March, 2004.

[Serghuita, 2004c] Private Communication, April, 2004.

[Serghuita, 2004d] Private Communication, May, 2004.

[Stammler, 1995] R. Stammler, SCANDPOWER A/S. (1995). HELIOS Methods HELIOS documentation Rev. No. 2.

[Whitlock, 1995] Whitlock, J.J., Garland, W.J., & Milgram, M.S. 1995). Effects Contributing to Positive Coolant Void Reactivity in CANDU. Transactions of the American Nuclear Society, 72, 329-330.

[Yu, 2002] Yu, S. (2002). An Overview of the ACR Design. Retrieved November 20, 2003, from U.S. Nuclear Regulatory Commission Web Site: http://www.nrc.gov/reactors/new-licensing/license-reviews/design-cert/acr-700.html/

Acknowledgements / Disclaimers

The authors would like to acknowledge the assistance of the U.S. NRC staff and the Canadian Nuclear Safety Commission staff during the course of this work. In particular, the extensive discussions and guidance of Don Carlson from the U.S. NRC and Dumitru Serghuita from the CNSC were instrumental in designing the numerical models developed in this work and in understanding the physics of ACR Voiding. However, this work does not represent an official endorsement by either the U.S. NRC or CNSC of the results and conclusions in this report.

Appendix A

Analysis of the Reactivity Contribution of Dysprosium Isotopes to the ACR-700 Coolant Void Reactivity

INTRODUCTION

Because of the importance of Dysprosium to the overall CVR, a study was performed to isolate the reactivity contributions of each specific Dysprosium isotope. A particular concern in the CVR analysis is the uncertainty in the Dysprosium ENDF/B-VI cross section data and the propagation of the cross section uncertainties into the prediction of the CVR. In the analysis here, the specific contributions to the CVR were determined for each dysprosium isotope and compared with results reported by AECL.

DESCRIPTION OF THE MODEL

The lattice code HELIOS 1.7, which uses the cross section library ENDF/B-VI rev. 3 [3], was used to model the ACR-700 fuel lattice using specifications provided by AECL [2]. The lattice model is depicted in Figure 1.

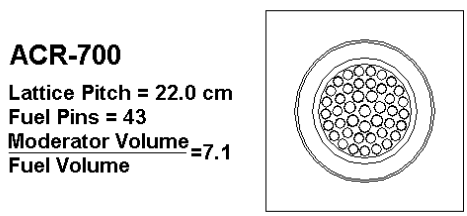

Fig. 1. ACR-700 Fuel Lattice

The HELIOS calculations were performed using 45 neutron energy groups and the lattice was depleted to 10MWd/kgU. Calculations simulating a 0% voiding (Cooled) and instantaneous 100% voiding (Voided) of the coolant were performed for both fuel designs. The necessary edits were performed in HELIOS to include the average macroscopic fission and absorption cross-sections defined over the entire lattice for several isotopes of uranium, plutonium, hydrogen, and dysprosium. Using the average neutron flux for the lattice, reaction rates and the specific contribution of each isotope to the overall CVR were calculated. A more detailed study was also performed to evaluate the sensitivity by energy group for each dysprosium isotope.

The means of calculating each isotopic contribution to the overall CVR was chosen to be as consistent as possible with the methods used by AECL [1]. The specific contribution of each isotope was calculated using the following formulas:

$$f_{ab\,i} = \text{Absorption Fraction} = \frac{\text{Isotope Absorption Reaction Rate}}{\text{Total Absorption Reaction Rate}} \quad (1)$$

$$f_{nf\,i} = \text{Nu Fission Fraction} = \frac{\text{Isotope Fission Reaction Rate}}{\text{Total Absorption Reaction Rate}} \quad (2)$$

$$f_{nf\,i} - f_{ab\,i} = \text{Net Yield} \quad (3)$$
$$= \text{Nu Fission Fraction-Absorption Fraction}$$

$$k_{inf}\ (\text{Based on Listed Isotopes}) = \frac{\sum_{1}^{N\,Isotopes} f_{nf\,i}}{\sum_{1}^{N\,Isotopes} f_{ab\,i}} \quad (4)$$

$$\Delta\rho_{Total} = \text{Total Reactivity Change From Isotopes} \quad (5)$$
$$= 1 - \frac{1}{k_{inf}}$$

$$\Delta\rho_i = \text{Isotope Reactivity Contribution} \quad (6)$$
$$= \Delta\rho_{Total} \frac{f_{nf\,i} - f_{ab\,i}}{\sum_{1}^{N\,Isotopes} (f_{nf\,i} - f_{ab\,i})}$$

It should be noted that because of space limitations the direct values calculated using equations 1 through 5 are not included in this summary, but their overall products, the isotope reactivity contribution $\Delta\rho_i$, are provided in the Isotope Contribution section below.

ISOTOPE CONTRIBUTIONS

The following isotope reactivity contributions ($\Delta\rho_i$) results were obtained for each isotope:

TABLE I. Contribution to k_{eff} by Isotope

Nuclide	AECL [1] (Cooled) Reactivity (mk)	HELIOS (Cooled) Reactivity (mk)	AECL [1] (Voided) Reactivity (mk)	HELIOS (Voided) Reactivity (mk)
U235	271.2	276.8	281.3	280.6
U238	-194.0	-204.0	-209.5	-217.8
Pu239	175.3	170.1	163.9	160.0
Pu240	-31.6	-30.6	-32.0	-31.5
Pu241	22.9	19.7	21.3	18.3
Pu242	-0.4	-0.3	-0.5	-0.5
H1 (Coolant)	-31.5	-29.2	0.0	-2.7
Dy160	-0.5	-0.4	-0.7	-0.6
Dy161	-5.1	-4.1	-7.2	-5.4
Dy162	-4.4	-3.8	-5.6	-4.3
Dy163	-4.1	-3.9	-6.0	-5.3
Dy164	-14.2	-11.5	-19.4	-13.1
Dy(Total)	-28.3	-23.6	-38.9	-28.6
Total (Isotopes)	183.6	178.8	185.6	177.9

TABLE II. Contribution to Lattice Coolant Void Reactivity by Isotope

Nuclide	AECL [1] Reactivity (mk)	HELIOS Reactivity (mk)
U235	10.1	3.9
U238	-15.5	-13.7
Pu239	-11.4	-10.1
Pu240	-0.4	-0.9
Pu241	-1.6	-1.3
Pu242	-0.1	-0.2
H1(Coolant)	31.5	26.4
Dy160	-0.2	-0.2
Dy161	-2.1	-1.2
Dy162	-1.2	-0.6
Dy163	-1.9	-1.4
Dy164	-5.2	-1.6
Dy(Total)	-10.6	-5.0
Total(Isotopes)	2.0	-0.9
Others Isotopes	-4.8	-4.7
Total	-2.8	-5.6

As indicated in Tables I and II, the overall trend in the results calculated with HELIOS appear to be reasonably consistent with the results reported by AECL. However, there are some noticeable differences in the contribution of specific Dysprosium isotopes. In particular, the negative contribution from Dysprosium-164 predicted by HELIOS is about a factor of 3 smaller than that reported by AECL

.

The energy spectrum was divided into twelve energy groups into to isolate the energy dependence of the CVR. The difference in the voided and coolant absorption rates of Dy is summarized in Table III and shown in Figure 2.

TABLE III.
Dysprosium Isotopic Change in Absorption Fraction [$f_{ab\ i}$] by Energy Group [Voided – Cooled]

Energy Range [eV]	Dy 160	Dy 161	Dy 162	Dy 163	Dy 164	Dy Total
2E+7 - 130.1	2.2E-5	2.2E-4	9.5E-5	1.5E-4	4.2E-5	0.05%

130.1 – 78.9	5.9E-6	5.7E-5	4.0E-6	3.4E-5	1.9E-7	0.01%
78.9 – 47.9	7.8E-6	4.6E-5	1.8E-4	6.6E-5	6.2E-8	0.03%
47.9 – 29.0	8.0E-6	3.5E-5	3.7E-7	7.5E-6	7.7E-8	0.01%
29.0 – 13.7	1.2E-5	8.3E-5	1.1E-6	1.3E-4	3.9E-7	0.02%
13.7 - 7.3	6.6E-5	3.9E-5	1.7E-5	2.0E-6	1.9E-6	0.01%
7.3 - 5.0	-6.8E-8	-6.3E-7	-1.7E-4	-1.4E-7	-4.8E-7	0.08%
5.0 - 3.9	8.0E-8	4.6E-5	8.8E-5	5.7E-7	1.9E-6	0.26%
3.9 - 2.4	8.6E-7	3.5E-4	8.1E-5	1.4E-5	1.8E-5	0.22%
2.4 - 1.0	4.3E-5	3.1E-5	5.4E-5	9.8E-4	5.7E-5	0.26%
1.0 - .1	9.9E-8	-3.0E-5	-9.0E-6	9.7E-6	-1.8E-4	0.22%
.1 - 0	4.8E-6	3.4E-4	2.2E-4	1.4E-4	1.8E-3	0.25%
Total	0.02%	0.12%	0.06%	0.15%	0.17%	0.52%

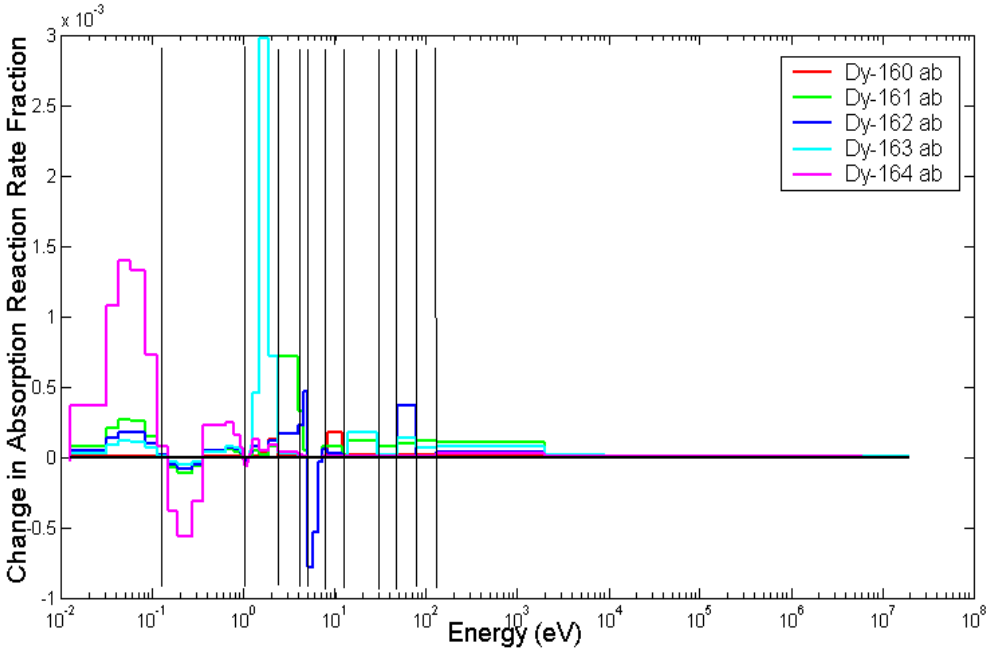

Figure 2 Changes Dysprosium Absorption by Energy

As indicated in Table III and Figure 2, the effect of dysprosium absorption on the CVR does not appear to play a significant role at energies higher than about 5eV. It is also apparent that the Dysprosium-164 sensitivity is the largest. As indicated in Table III, after voiding the overall amount of absorption increases for all the dysprosium isotopes over all defined energy ranges, especially at energies below 5eV.

CONCLUSION

The results reported here with the HELIOS lattice code appear to be reasonably consistent with those previously reported by AECL [1]. The importance of specific Dysprosium isotopes to the negative CVR in the ACR-700 lattice was determined and the energy group-wise sensitivities will provide useful insight into more detailed studies into the overall uncertainty of the ACR-700 CVR.

REFERENCES

References that include an NRC ADAMS Accession Number are available in the U.S. Nuclear Regulatory Commission's Agency wide Document Access and Management System (ADAMS), which is accessible from the Public Electronic Reading Room at: www.nrc.gov/reading-rm.html. Select Web-Based Access and search for the Accession Number.

1. Chan, P., Coolant Void Reactivity Components in ACR Lattice, Presentation at 2nd Meeting of NRC PIRT Panel on ACR-700 Neutronics, December 11-12, 2003.
2. Atomic Energy of Canada Limited, ACR-700 Technical Description, (10810-01371-TED-001 Revision 0), Ontario, Canada: AECL, June 2003, (NRC ADAMS Accession Number ML032030391).
3. J. J. Casal, R. J. J. Stamm'ler, E. A. Villario, and A. A. Ferri, "HELIOS: Geometric capabilities of a new fuel-assembly program," Proc. Int. Topl. Mtg. Advances in Mathematics, Computations, and Reactor Physics, Pittsburgh, PA, April 28 May 2 (1991), Vol. 2, p 10.2.11-13.